Electronic Supporting Information for

Spin Crossover Fe(II) Complexes of a Cross-Bridged Cyclam Derivative

*Bohuslav Drahoš and Zdeněk Trávníček**

Department of Inorganic Chemistry & Regional Centre of Advanced Technologies and Materials, Faculty of Science, Palacký University, 17. listopadu 12, 771 46 Olomouc, Czech Republic

*zdenek.travnicek@upol.cz

Figure S1 $^{1}H–^{1}H$ gs-COSY NMR spectrum of **L**.

Figure S2 $^{1}H–^{13}C$ gs-HMQC NMR spectrum of **L**.

Figure S3a,b $^{1}H–^{13}C$ gs-HMBC NMR spectra of **L**.

Figure S4 Comparison of TG/DSC curves measured for the studied Fe^{II} complexes **1**·H_2O, **2**·$4H_2O$, **3** $0.5CH_3CN$ and **4**·CH_3OH.

Figure S5 Comparison of IR spectra of the studied cross-bridged cyclam ligand **L** and its Fe^{II} complexes **1**·H_2O, **2**·$4H_2O$, **3** and **4**·CH_3OH.

Figure S6 The powder X-ray diffraction patterns of **1**·H_2O (*top*)**,** **2**·$4H_2O$ (*middle*), and theoretically calculated pattern of **2**·$1.5H_2O$ from single-crystal X-ray data at 120 K (*bottom*).

Figure S7 The powder X-ray diffraction patterns of freshly prepared **3**·$0.5CH_3CN$ (*top*), **3** (*middle*), theoretically calculated pattern from single-crystal X-ray data of **3** at 293 K (*middle*) and **4**·CH_3OH (*bottom*).

Figure S8 The molecular structure of the complex [Fe(**L**)][$FeCl_4$]$_2$ (**1a**).

Figure S9 The molecular structure of the complex [Fe(**L**)](BPh_4)$_2$ (**4**).

Figure S10 The asymmetric unit of **2**·$1.5H_2O$, showing two crystallographically independent molecules of the $[Fe(L)]^{2+}$ cation. Hydrogen atoms, chloride anions and crystal water molecules were omitted for clarity.

Figure S11 Part of the crystal structure of **2**·$1.5H_2O$, showing the O–H···Cl hydrogen bonds and C–$H_{aromatic}$···Cl/O non-covalent contacts (red dashed lines). Hydrogen atoms not involved into the non-covalent interactions were omitted for clarity.

Figure S12 Part of the crystal structure of **3** (120 K), showing the $C–H_{aromatic}\cdots F$ non-covalent contacts (red dashed lines). Hydrogen atoms not involved in the non-covalent interactions were omitted for clarity.

Figure S13 Thermal dependence of the derivative of $\chi_m T$ product for complexes **1**·H_2O, **3** and **4**·CH_3OH.

Table S1 Crystal data and structure refinements for complex [Fe(**L**)][$FeCl_4$]$_2$ (**1a**).

Table S2 Selected bond lengths (Å) and angles (°) for complex **1a**.

Table S3 Selected non-covalent contacts (Å, °) for complex **1a**.

Table S4 Selected non-covalent contacts (Å, °) for complexes **2**·1.5H_2O.

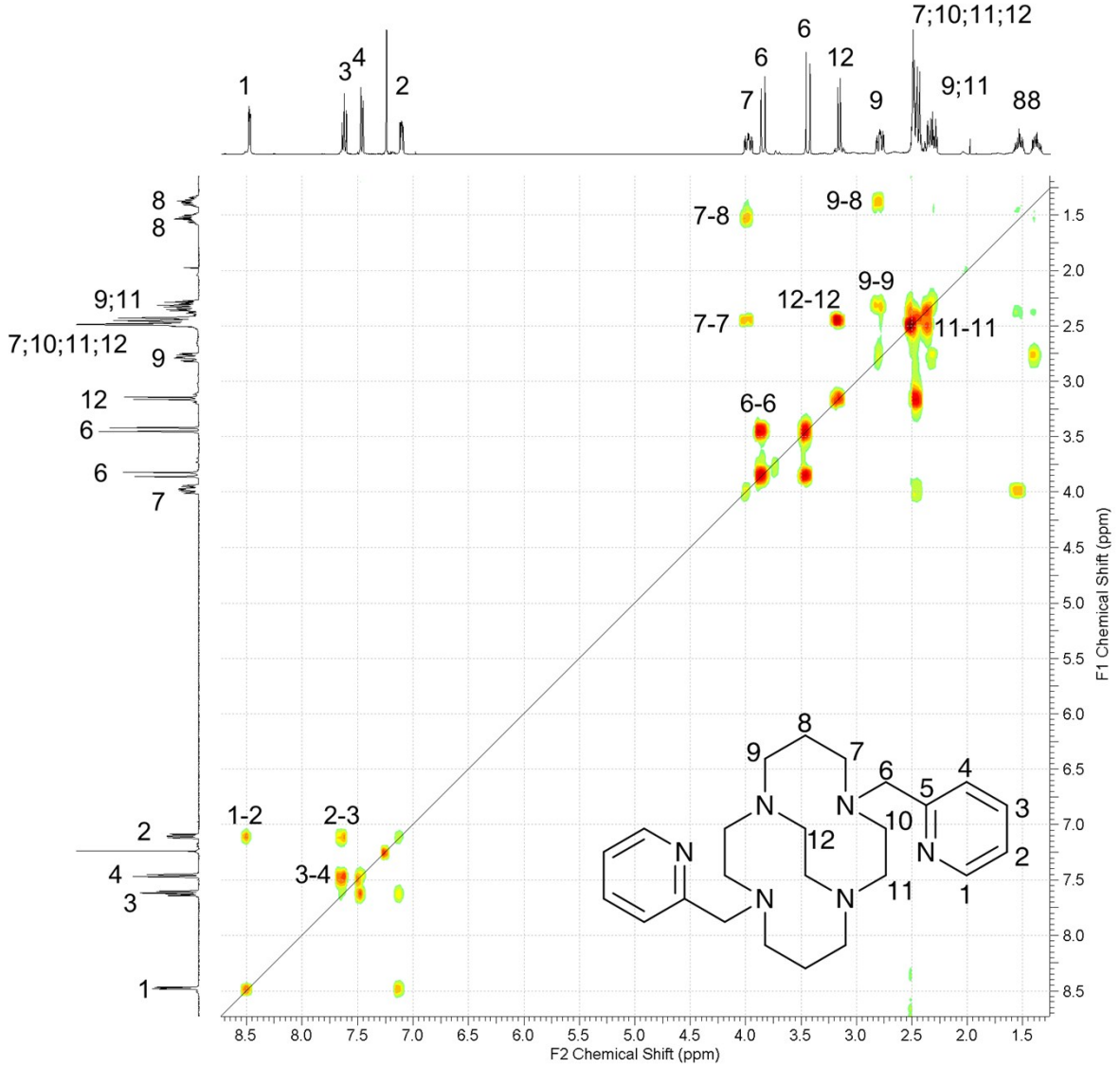

Figure S1 ^{1}H–^{1}H gs-COSY NMR spectrum (400MHz, $CDCl_3$) of **L** (4,11-bis((pyridin-2-yl)methyl)-1,4,8,11-tetraaza-bicyclo[6.6.2]hexadecane) with a residual peak of $CHCl_3$ at 7.26 ppm.

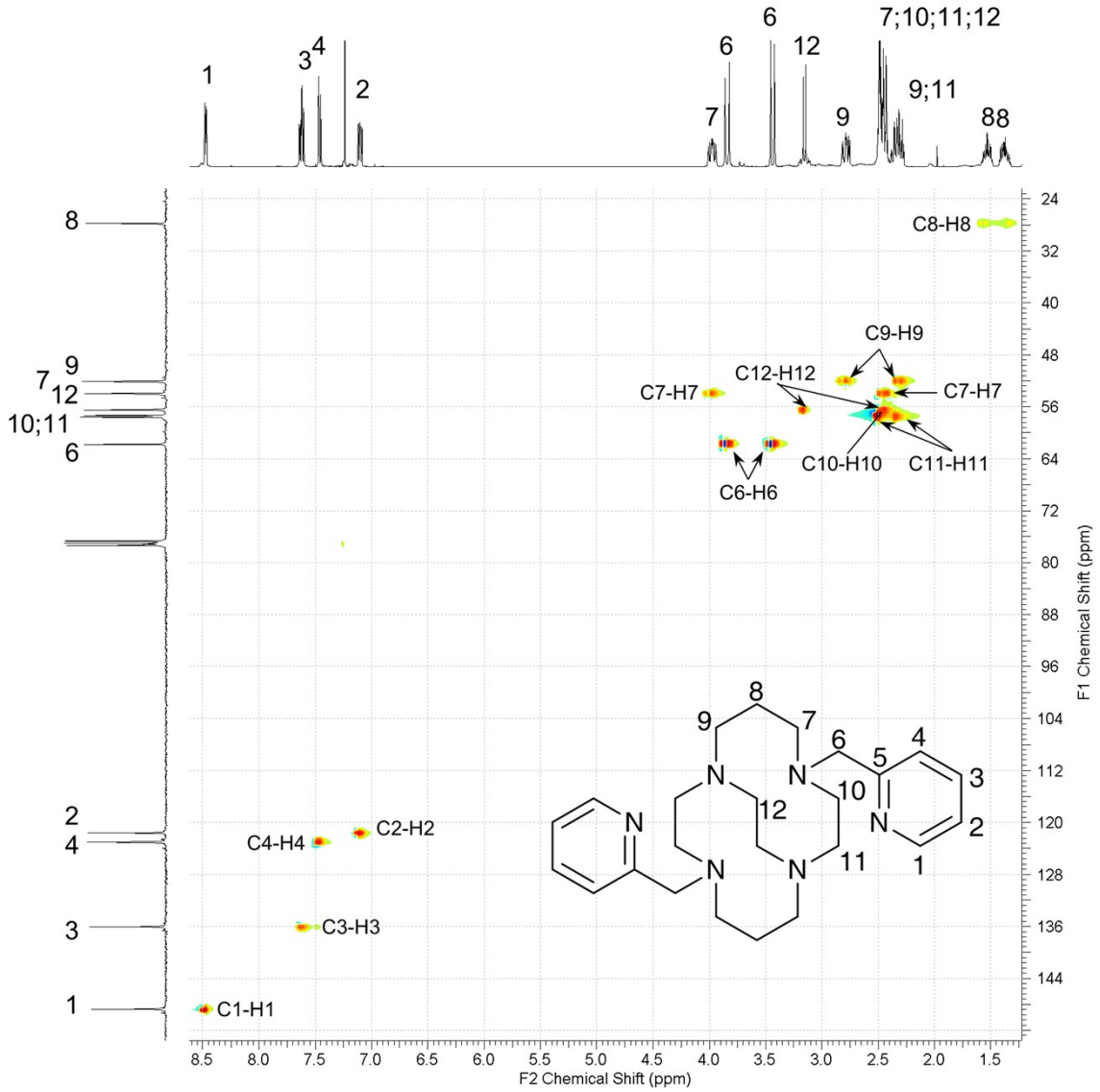

Figure S2 ^{1}H–^{13}C gs-HMQC NMR spectrum (400MHz, $CDCl_3$) of **L** (4,11-bis((pyridin-2-yl)methyl)-1,4,8,11-tetraaza-bicyclo[6.6.2]hexadecane) with a residual peak of $CHCl_3$ at 7.26 ppm (^{1}H) and $CDCl_3$ at 77.2 ppm (^{13}C).

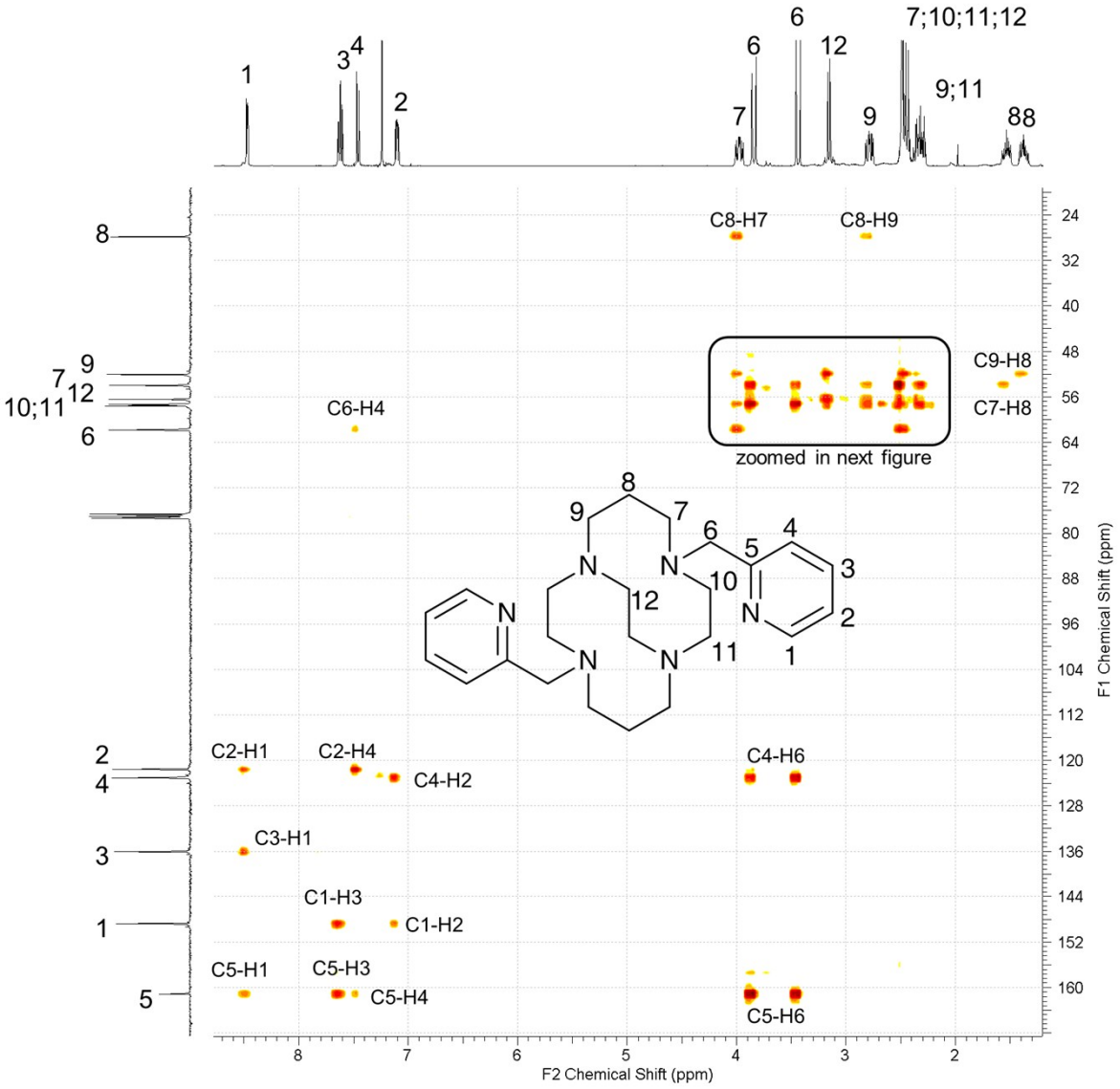

Figure S3a ^{1}H–^{13}C gs-HMBC NMR spectrum (400MHz, $CDCl_3$) of **L** (4,11-bis((pyridin-2-yl)methyl)-1,4,8,11-tetraaza-bicyclo[6.6.2]hexadecane) with a residual peak of $CHCl_3$ at 7.26 ppm (^{1}H) and $CDCl_3$ at 77.2 ppm (^{13}C).

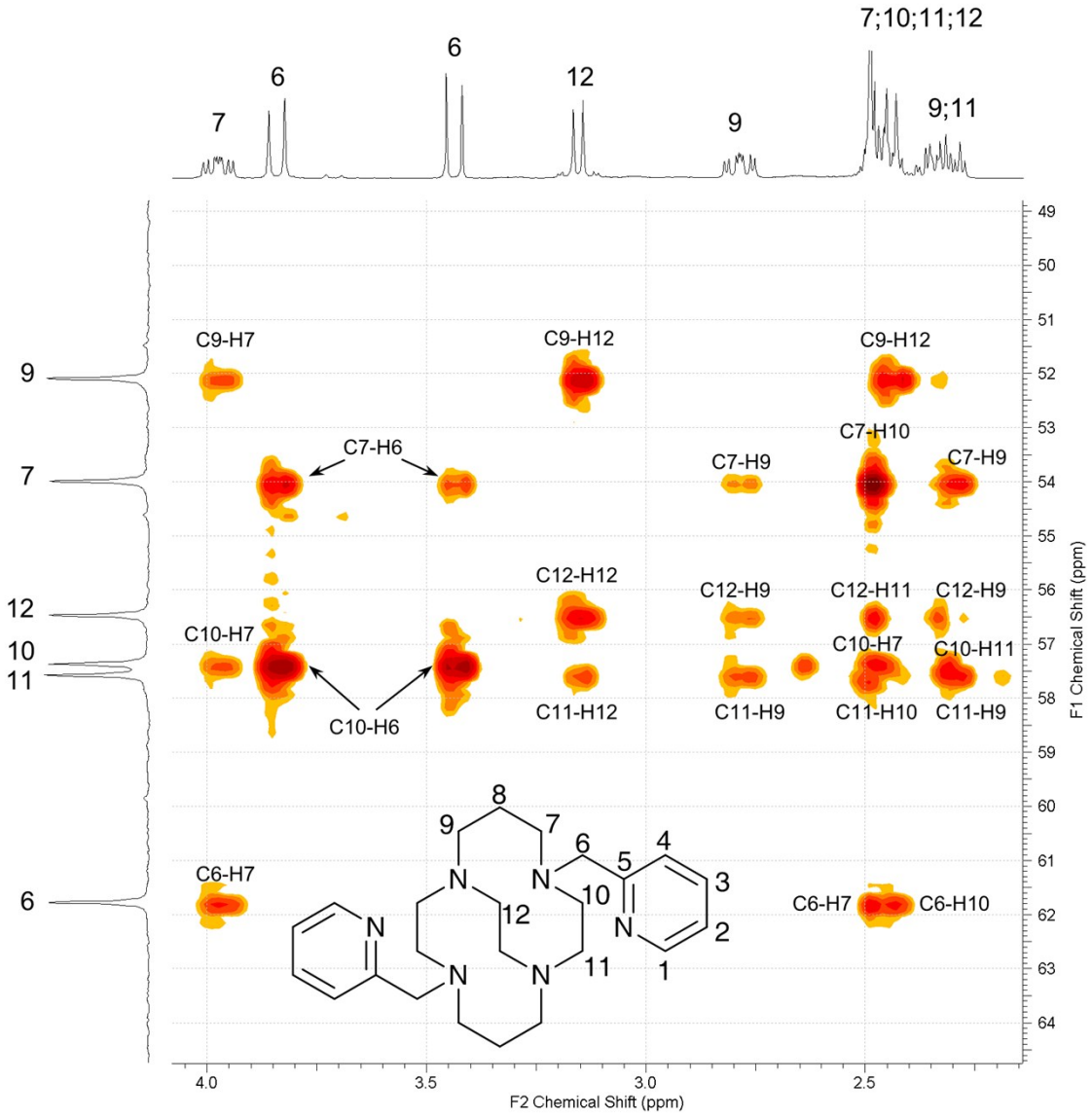

Figure S3b Expansion of the $^{1}H–^{13}C$ gs-HMBC NMR spectrum (400MHz, $CDCl_3$) of **L** (4,11-bis((pyridin-2-yl)methyl)-1,4,8,11-tetraaza-bicyclo[6.6.2]hexadecane).

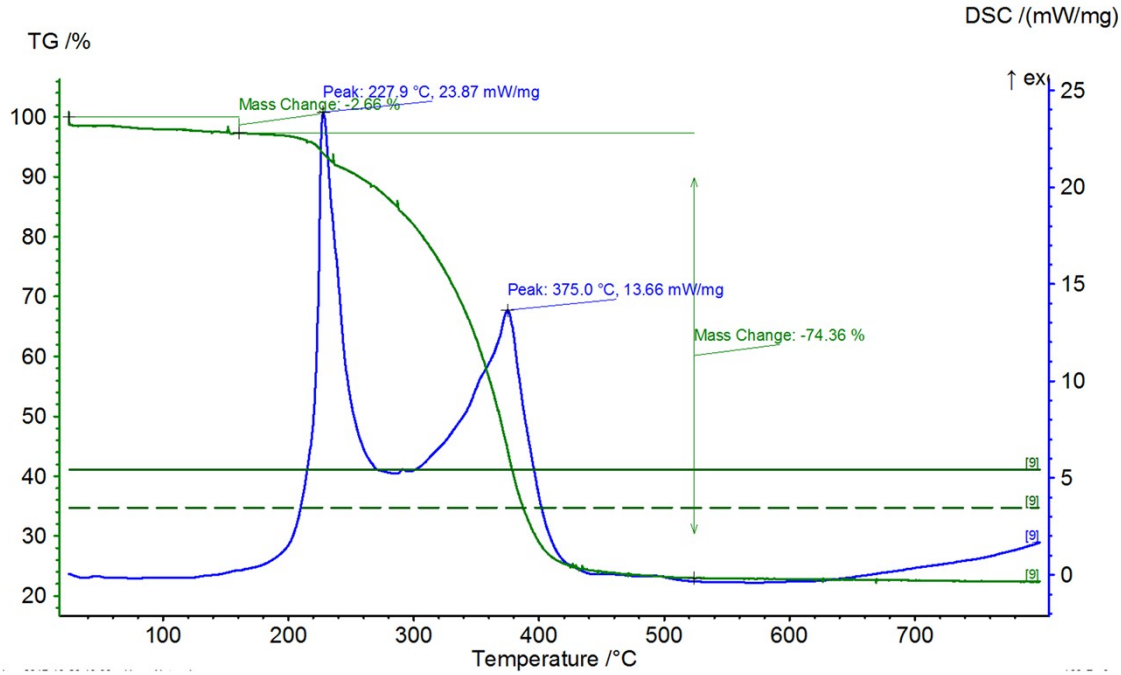
TG /%
DSC /(mW/mg)
↑ exo
Peak: 227.9 °C, 23.87 mW/mg
Mass Change: -2.66 %
Peak: 375.0 °C, 13.66 mW/mg
Mass Change: -74.36 %
[9]
[9]
[9]
[9]
Temperature /°C

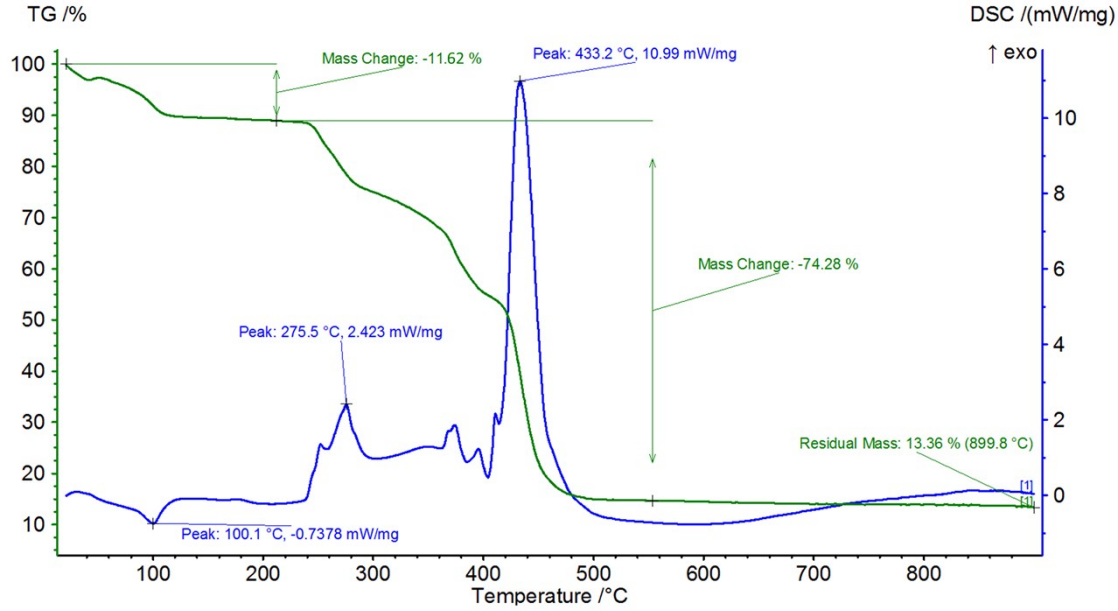
TG /%
DSC /(mW/mg)
↑ exo
Mass Change: -11.62 %
Peak: 433.2 °C, 10.99 mW/mg
Mass Change: -74.28 %
Peak: 275.5 °C, 2.423 mW/mg
Residual Mass: 13.36 % (899.8 °C)
[1]
[1]
Peak: 100.1 °C, -0.7378 mW/mg
Temperature /°C

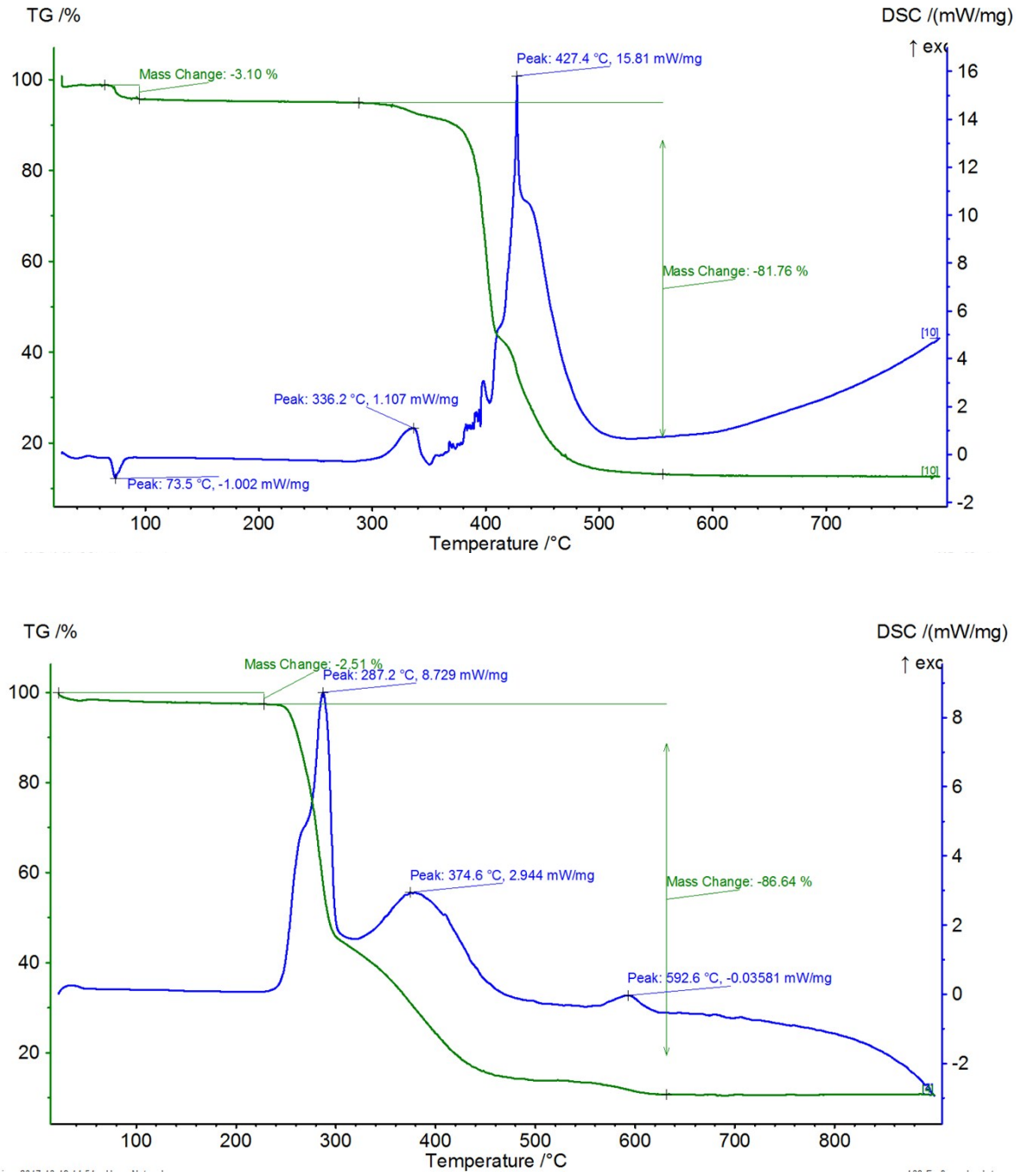

Figure S4 Comparison of TG/DSC curves measured for the studied Fe^{II} complexes **1**·H_2O, **2**·$4H_2O$, **3** $0.5CH_3CN$ and **4** CH_3OH (*from the top to the bottom*).

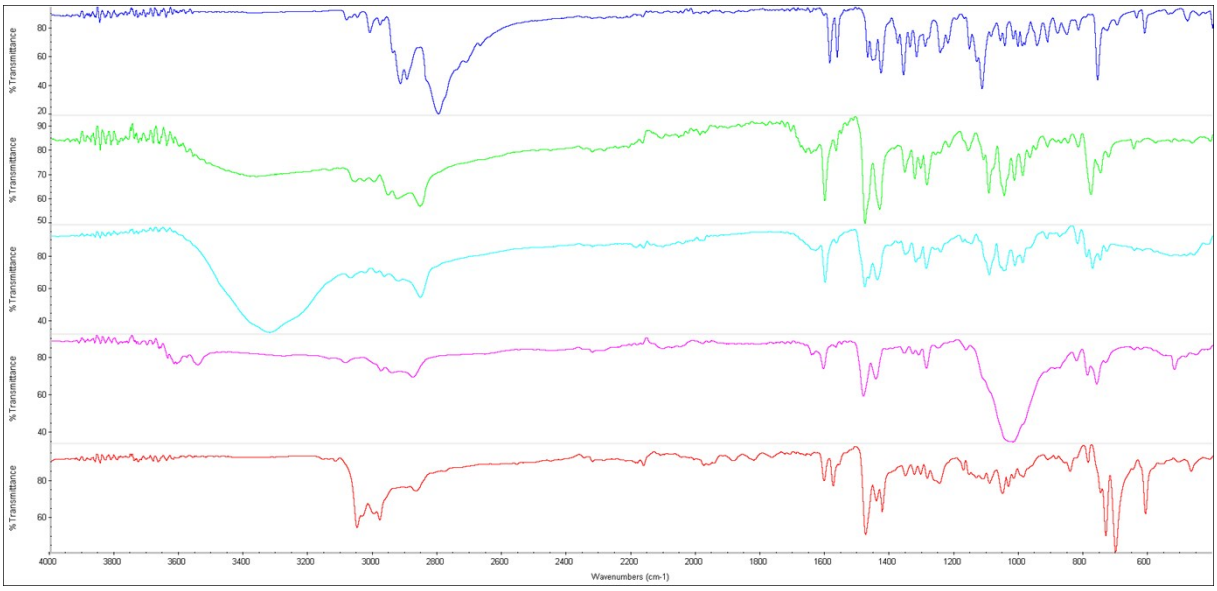

Figure S5 Comparison of IR spectra of the cross-bridged cyclam ligand **L** and its Fe^{II} complexes **1**·H_2O, **2**·$4H_2O$, **3** and **4**·CH_3OH (*from the top to the bottom*).

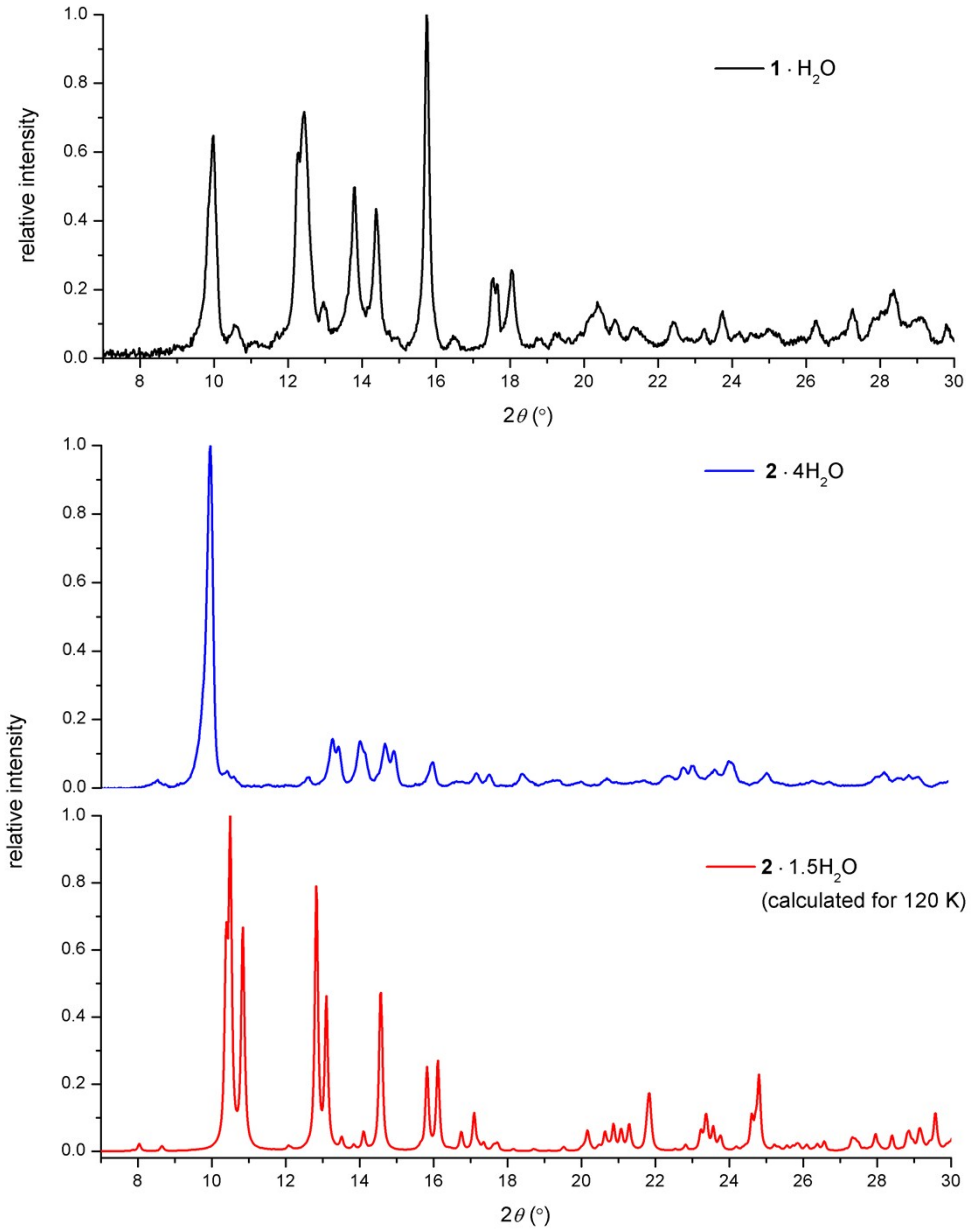

Figure S6 The powder X-ray diffraction patterns of **1**·H_2O (*top*)**,** **2**·4H_2O (*middle*), and theoretically calculated pattern of **2**·1.5H_2O from single-crystal X-ray data at 120 K (*bottom*).

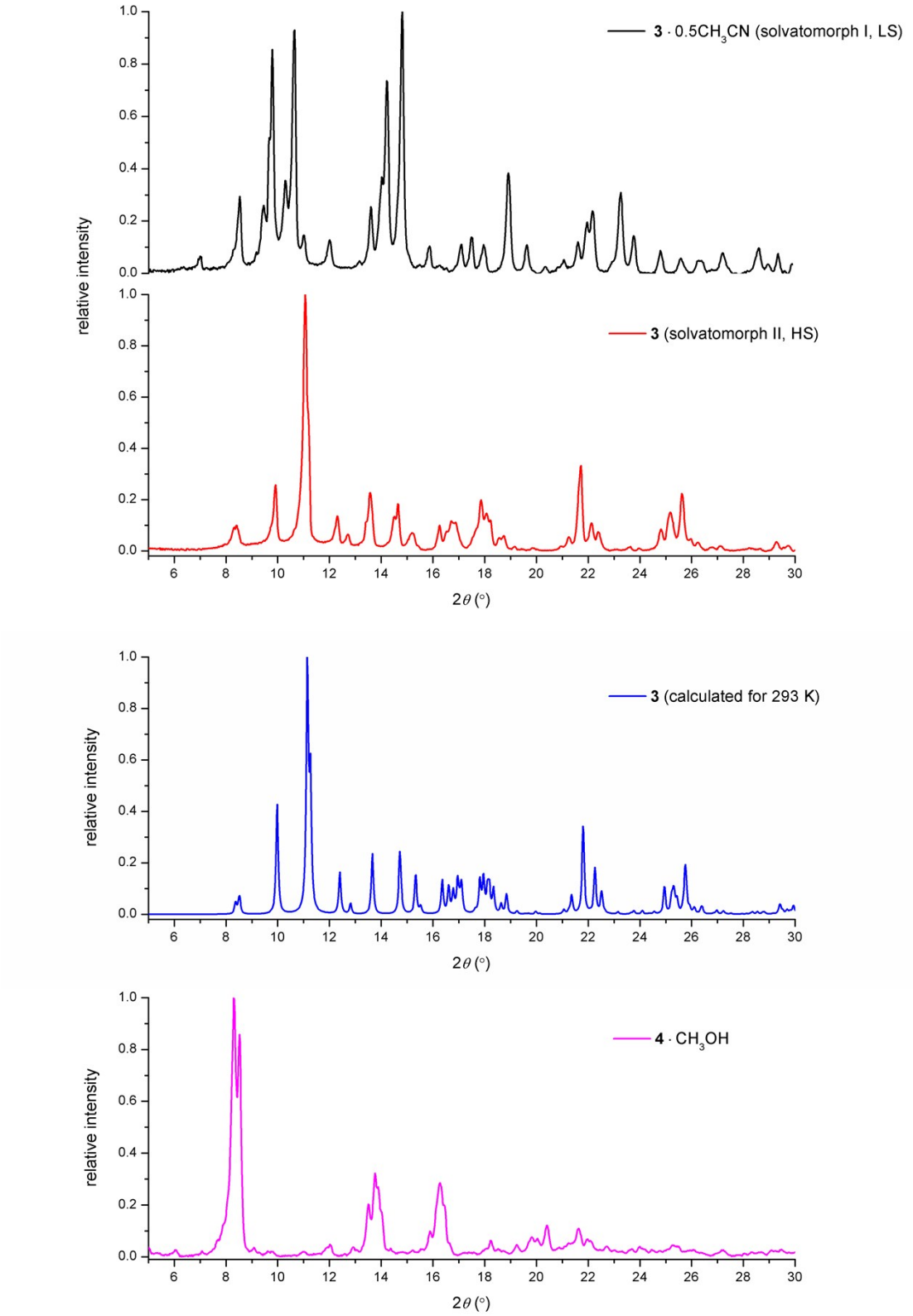

Figure S7 The powder X-ray diffraction patterns of freshly prepared **3**·0.5CH_3CN (*top*), **3** (*middle*), theoretically calculated pattern from single-crystal X-ray data of **3** at 293 K (*middle*) and **4**·CH_3OH (*bottom*).

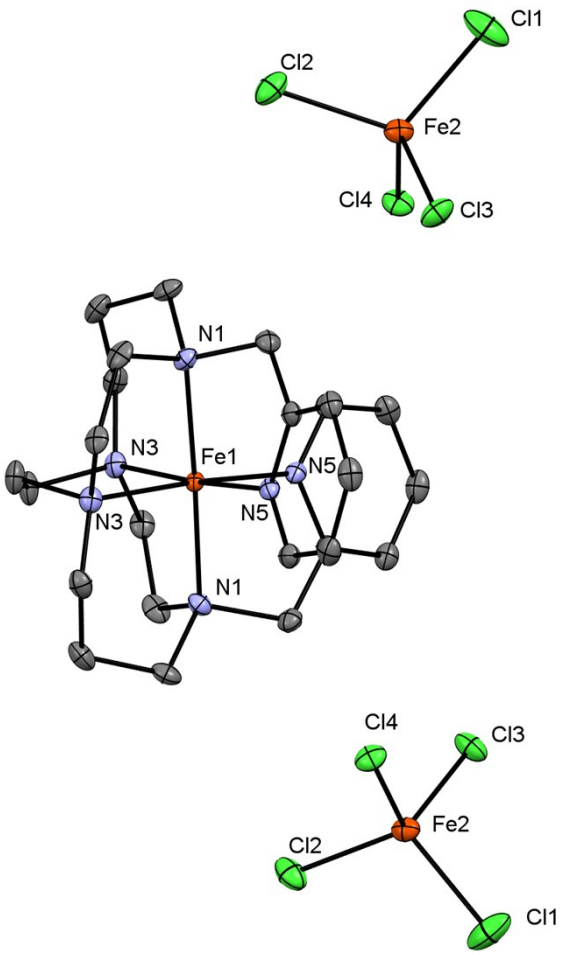

Figure S8 The molecular structure of the complex [Fe(**L**)][$FeCl_4$]$_2$ (**1a**). Non-hydrogen atoms are drawn as thermal ellipsoids at the 50% probability level. Hydrogen atoms were omitted for clarity.

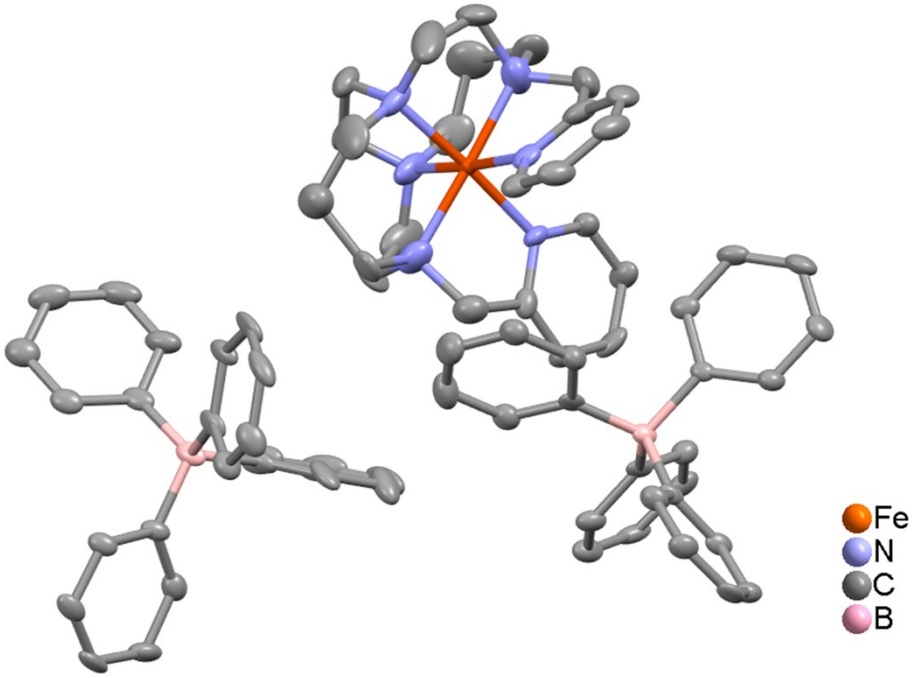

Figure S9 The molecular structure of the complex [Fe(**L**)]$(BPh_4)_2$ (**4**). Non-hydrogen atoms are drawn as thermal ellipsoids at the 50% probability level. Hydrogen atoms were omitted for clarity. The structure was determined based on the X-ray data of a poor quality [*R*(int) = 0.1134] and thus the obtained results do not fulfil requirements needed for their publication (Final *R* indices based on 25 948 data, I>2σ(I), *R*1 = 0.1088, w*R*2 = 0.2493). However, the composition and molecular structure of **4** is clearly seen. Moreover, the Fe–N bond lengths are within the interval of 2.030-2.072 Å, supporting the presence of the Fe(II) atom in the low-spin state at 120 K.

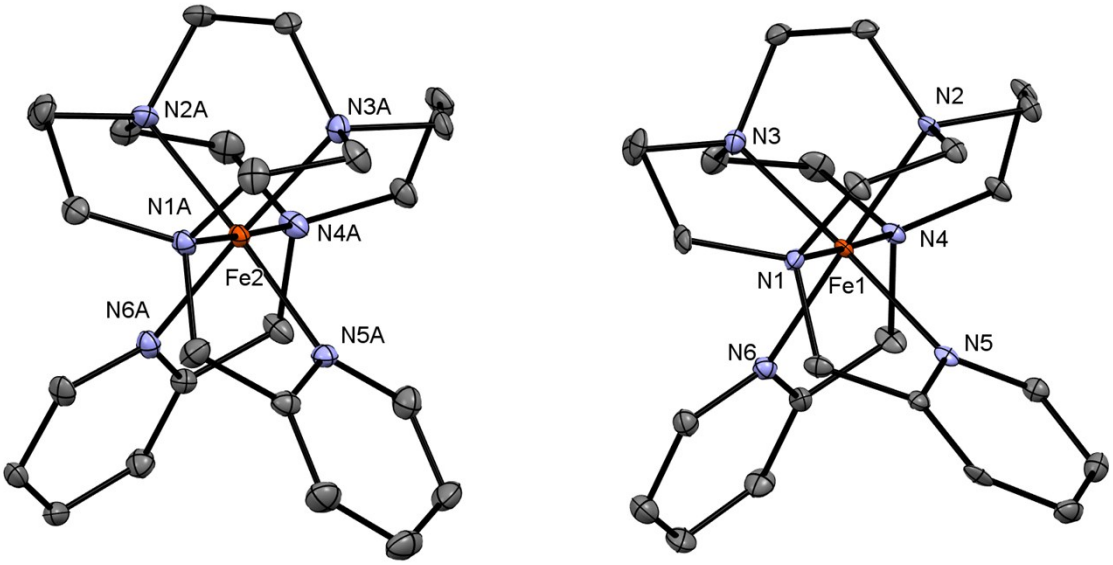

Figure S10 The asymmetric unit of **2**·1.5H_2O showing two crystallographically independent molecules of the $[Fe(L)]^{2+}$ cation. Hydrogen atoms, chloride anions and crystal water molecules were omitted for clarity.

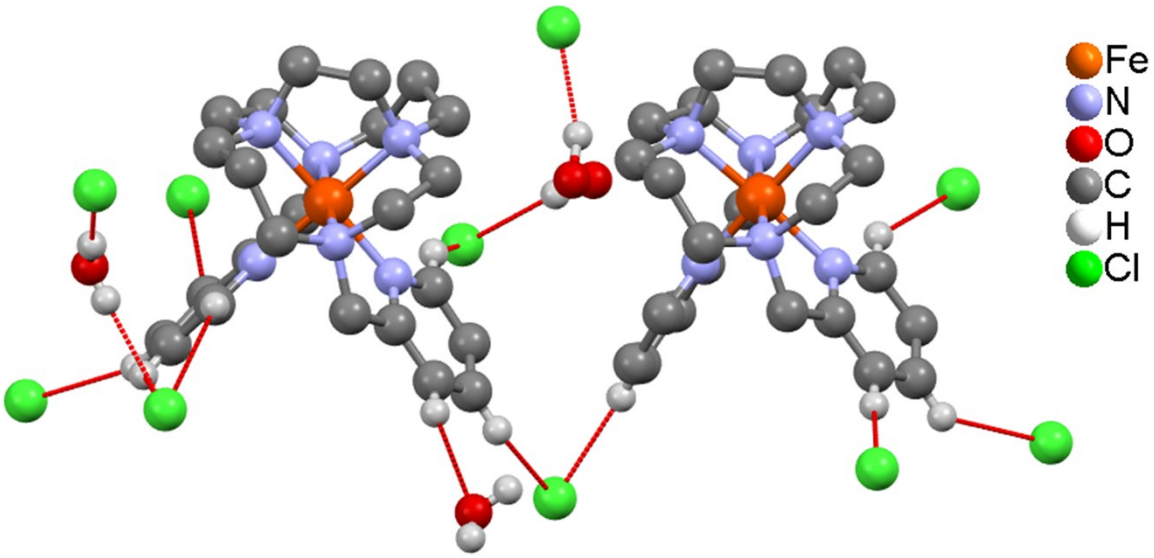

Figure S11 Part of the crystal structure of **2**·1.5H_2O, showing the O–H···Cl hydrogen bonds and C–$H_{aromatic}$···Cl/O non-covalent contacts (red dashed lines). Hydrogen atoms not involved into the non-covalent interactions were omitted for clarity.

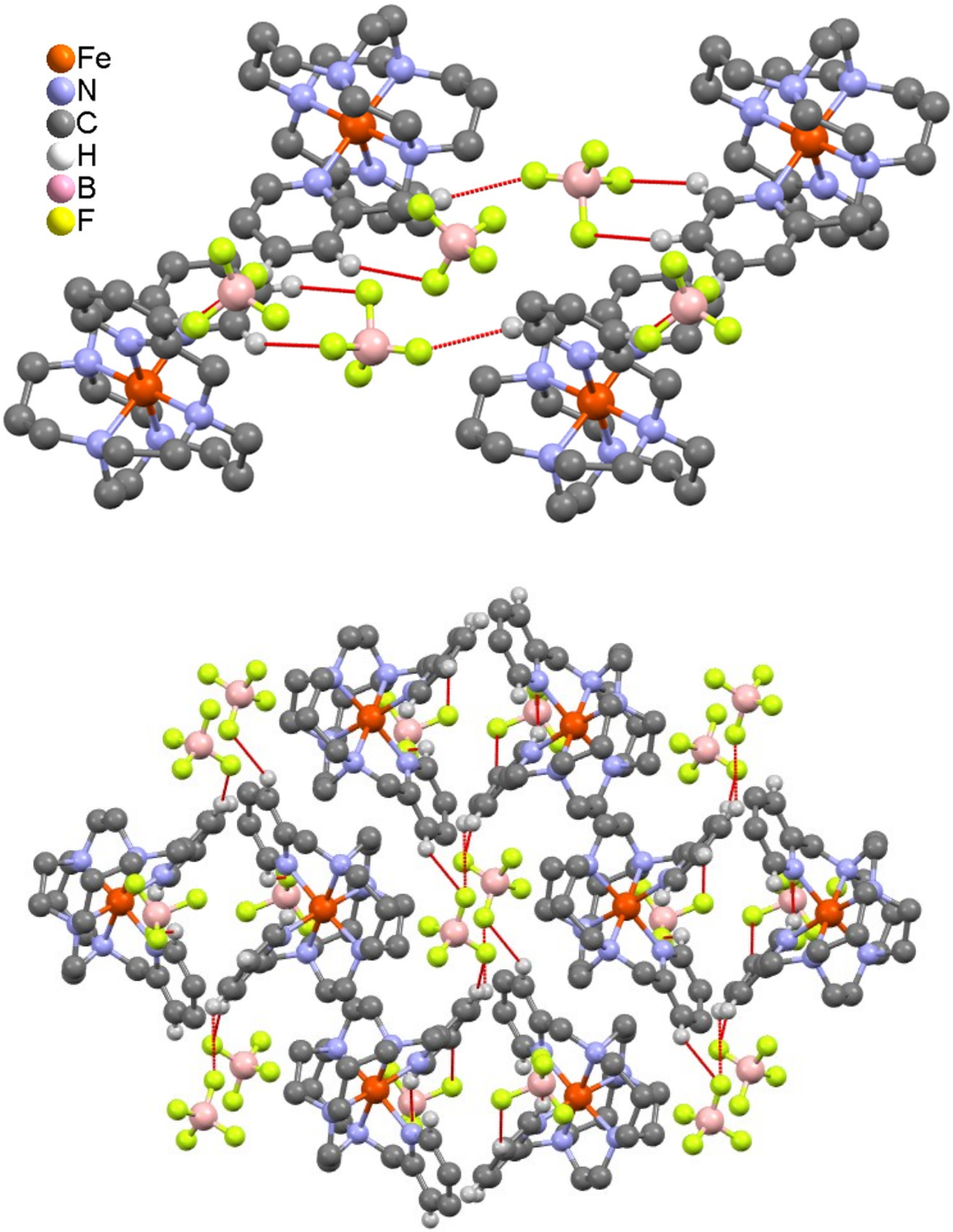

Figure S12 Part of the crystal structure of **3** (120 K), showing the C–$H_{aromatic}$···F non-covalent contacts (red dashed lines). Hydrogen atoms not involved in the non-covalent interactions were omitted for clarity.

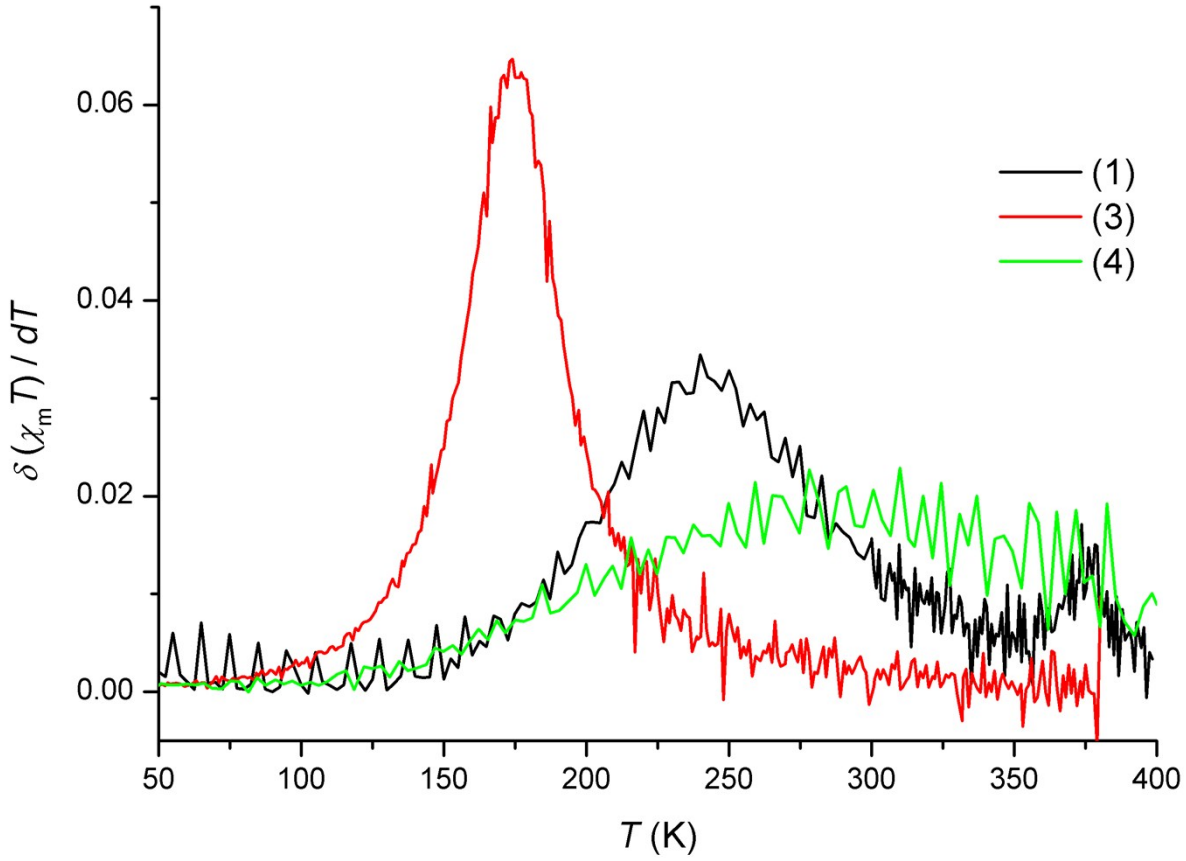

Figure S13 Thermal dependence of the derivative of $\chi_m T$ product for complexes **1**·H_2O (*black*), **3** (*red*) and **4** CH_3OH (*green*).

Table S1 Crystal data and structure refinements for complex [Fe(**L**)][$FeCl_4$]$_2$ (**1a**).

Compound	**1a**
Formula	$C_{24}H_{36}Cl_8Fe_3N_6$
M_r	859.74
Temperature (K)	120(2)
Wavelength (Å)	0.71073
Crystal system	Monoclinic
Space group	C2/c
a (Å)	21.7383(15)
b (Å)	8.0208(5)
c (Å)	20.5678(14)
α (°)	90
β (°)	112.832(2)
γ (°)	90
V, Å^3	3305.2(4)
Z	4
D_{calc}, g cm^{-3}	1.728
μ, mm^{-1}	1.974
F(000)	1744
θ range for data collection (°)	2.015–24.997
Refl. collected	20871
Independent refl.	2914
R(int)	0.0545
Data/restrains/parameters	2914 / 0 / 186
Completeness to θ (%)	99.9
Goodness-of-fit on F^2	0.956
$R1$, w$R2$ ($I>2\sigma(I)$[a]	0.0277; 0.0606
$R1$, w$R2$ (all data)[a]	0.0393; 0.0639
Largest diff. peak and hole / A^{-3}	0.718 and –0.433
CCDC	1828318

[a] $R_1 = \Sigma(||F_o| - |F_c||) / \Sigma|F_c|$; $wR_2 = [\Sigma w(F_o^2 - F_c^2)^2 / \Sigma w(F_o^2)^2]^{1/2}$

Table S2 Selected bond lengths (Å) and angles (°) for complex **1a**.

Distances	
Fe–N(1)	2.090(2)
Fe–N(3)	2.045(2)
Fe–N(5)	2.044(2)
⟨Fe–N⟩	2.060
Angles	
N(5)-Fe(1)-N(5)$^{\#1}$	91.63(11)
N(5)-Fe(1)-N(3)	174.77(8)
N(5)$^{\#1}$-Fe(1)-N(3)	91.19(8)
N(5)-Fe(1)-N(3)$^{\#1}$	91.19(8)
N(5)$^{\#1}$-Fe(1)-N(3)$^{\#1}$	174.76(8)
N(3)-Fe(1)-N(3)$^{\#1}$	86.35(12)
N(5)-Fe(1)-N(1)	80.61(8)
N(5)$^{\#1}$-Fe(1)-N(1)	100.74(8)
N(3)-Fe(1)-N(1)	94.53(8)
N(3)$^{\#1}$-Fe(1)-N(1)	84.08(8)
N(5)-Fe(1)-N(1)$^{\#1}$	100.79(9)
N(5)$^{\#1}$-Fe(1)-N(1)$^{\#1}$	80.54(9)
N(3)-Fe(1)-N(1)$^{\#1}$	84.08(8)
N(3)$^{\#1}$-Fe(1)-N(1)$^{\#1}$	94.53(8)
N(1)-Fe(1)-N(1)$^{\#1}$	178.10(12)

Symmetry transformations used to generate equivalent atoms: $^{\#1}$ -x+1,y,-z+3/2

Table S3 Selected non-covalent contacts (Å, °) for complex **1a**.

D-H...A	d(D-H)	d(H...A)	d(D...A)	<(DHA)
C(3)-H(3B)...Cl(4)$^{\#2}$	0.99	2.84	3.561(3)	130.5
C(4)-H(4B)...Cl(3)$^{\#3}$	0.99	2.73	3.678(3)	159.7
C(4)-H(4A)...Cl(3)$^{\#4}$	0.99	2.83	3.776(3)	160.2
C(5)-H(5A)...Cl(2)$^{\#4}$	0.99	2.94	3.629(2)	127.3
C(7)-H(7A)...Cl(4)	0.95	2.84	3.512(3)	128.8

Symmetry transformations used to generate equivalent atoms: $^{\#1}$ -x+1,y,-z+3/2; $^{\#2}$ x,-y+1,z+1/2; $^{\#3}$ -x+1,y+1,-z+3/2; $^{\#4}$ x-1/2,y+1/2,z

Table S4 Selected non-covalent contacts (Å, °) for complex **2**·1.5H_2O.

D-H...A	d(D-H)	d(H...A)	d(D...A)	<(DHA)
C(1)-H(1B)...O(1)[#1]	0.99	2.42	3.369(4)	160.0
C(2)-H(2A)...Cl(3)[#2]	0.99	2.76	3.479(3)	130.1
C(3)-H(3A)...Cl(3)[#3]	0.99	2.92	3.744(3)	141.7
C(5)-H(5B)...Cl(1)	0.99	2.72	3.617(3)	151.5
C(6)-H(6B)...Cl(4)	0.99	2.67	3.632(3)	165.0
C(9)-H(9B)...Cl(2)	0.99	2.94	3.908(3)	167.2
C(9)-H(9A)...Cl(3)[#3]	0.99	2.92	3.722(3)	138.2
C(11)-H(11B)...Cl(2)[#2]	0.99	2.93	3.840(3)	153.9
C(11)-H(11A)...Cl(1)	0.99	2.93	3.799(3)	146.9
C(13)-H(13A)...O(2)[#4]	0.99	2.31	3.221(4)	153.3
C(16)-H(16A)...O(1)[#4]	0.95	2.50	3.398(4)	157.2
C(19)-H(19A)...Cl(1)	0.95	2.69	3.447(3)	137.5
C(21)-H(21A)...Cl(2)[#2]	0.95	2.84	3.653(3)	143.7
C(23)-H(23A)...Cl(3)	0.95	2.88	3.493(3)	123.7
C(24)-H(24A)...Cl(3)	0.95	2.82	3.473(3)	127.0
C(25)-H(25B)...Cl(1)[#3]	0.99	2.55	3.409(3)	144.4
C(26)-H(26B)...Cl(2)[#5]	0.99	2.75	3.590(3)	142.8
C(29)-H(29B)...Cl(4)[#6]	0.99	2.65	3.588(3)	158.2
C(30)-H(30A)...O(3A)	0.99	2.62	3.355(17)	131.3
C(30)-H(30A)...O(3B)	0.99	2.61	3.46(2)	144.5
C(33)-H(33A)...Cl(3)[#4]	0.99	2.82	3.771(3)	160.8
C(35)-H(35B)...Cl(4)[#7]	0.99	2.96	3.785(4)	141.5
C(40)-H(40A)...Cl(1)[#7]	0.95	2.67	3.591(3)	162.8
C(43)-H(43A)...Cl(4)[#6]	0.95	2.72	3.505(3)	140.3
C(48)-H(48A)...Cl(2)[#4]	0.95	2.97	3.641(3)	129.1
O(1)-H(1V)...Cl(3)[#3]	0.75(4)	2.55(4)	3.286(3)	171(4)
O(1)-H(1W)...Cl(2)	0.83(4)	2.42(4)	3.247(3)	177(3)
O(2)-H(2W)...Cl(2)	0.89(4)	2.30(4)	3.196(3)	179(3)
O(2)-H(2V)...Cl(3)	0.74(4)	2.51(4)	3.243(3)	172(4)
O(3A)-H(3V)...Cl(4)	1.08(4)	2.22(4)	3.187(13)	147(4)
O(3B)-H(3V)...Cl(4)	0.95(4)	2.22(4)	3.152(10)	168(4)
O(3A)-H(3W)...Cl(1)	0.77(4)	2.52(4)	3.243(13)	157(7)
O(3B)-H(3W)...Cl(1)	0.82(4)	2.52(4)	3.214(12)	144(6)

Symmetry transformations used to generate equivalent atoms: [#1] -x+1, -y, -z+1; [#2] -x+1, y-1/2, -z+1/2; [#3] x, -y+1/2, z+1/2; [#4] -x+1, y+1/2, -z+1/2; [#5] -x+1, -y+1, -z+1; [#6] -x, y+1/2, -z+1/2; [#7] x, y+1, z.